

IOS: INTER-OPERATOR SCHEDULER FOR CNN ACCELERATION

Yaoyao Ding^{*1} Ligeng Zhu² Zhihao Jia³ Gennady Pekhimenko¹ Song Han²

ABSTRACT

To accelerate CNN inference, existing deep learning frameworks focus on optimizing *intra-operator* parallelization. However, a single operator can no longer fully utilize the available parallelism given the rapid advances in high-performance hardware, resulting in a large gap between the peak performance and the real performance. This performance gap is more severe under smaller batch sizes. In this work, we extensively study the parallelism *between* operators and propose Inter-Operator Scheduler (IOS) to automatically schedule the execution of multiple operators in parallel. IOS utilizes dynamic programming to find a scheduling policy specialized for the target hardware. IOS consistently outperforms state-of-the-art libraries (e.g., TensorRT) by 1.1 to 1.5 \times on modern CNN benchmarks.

1 INTRODUCTION

Convolutional neural networks (CNNs) have achieved state-of-the-art performance across many tasks including computer vision (Krizhevsky et al., 2012; He et al., 2016), machine translation (Sutskever et al., 2014; Devlin et al., 2018), and game playing (Mnih et al., 2013; Silver et al., 2016). The success comes at the cost of growing computational requirements. The high demand for computation makes efficient inference more important in real deployment (Han et al., 2015; Chen et al., 2018; Jia et al., 2019a).

A common practice to improve the inference efficiency is parallelization. Deep learning frameworks such as TensorFlow (Abadi et al., 2016) and Pytorch (Paszke et al., 2017) exploit *intra-operator parallelism*, which parallelizes arithmetic operations within a *single* CNN operator (e.g., convolution). However, due to the rapid advances in high-performance hardware, intra-operator parallelism is no longer sufficient to obtain efficient resource utilization. As shown in Figure 1, the peak FP32 performance of a GPU has increased from 5.8 TFLOPs/s in 2013 to 15.7 TFLOPs/s in 2018 (shown in cyan). NVIDIA Tesla A100 even reaches a peak FP32 performance of 19.5 TFLOPs/s.

Meanwhile, there is a recent trend in CNN design to replace a single branch of convolutions with multiple branches of convolutions, which is advantageous due to increased model capacity under a fixed computation budget (Szegedy et al., 2016; Zoph et al.; Xie et al., 2019). As a result, the number of convolutions grows while the computation FLOPs

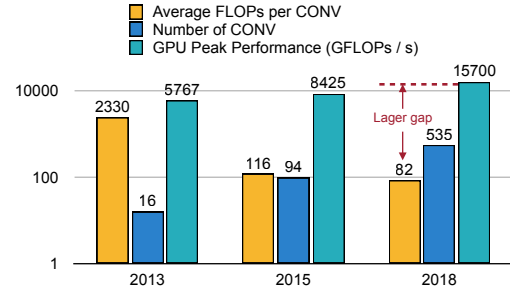


Figure 1. The trends of average computation per convolution, number of convolutions in a CNN and hardware peak performance. Device peak performance increases while average computation per convolution decreases, leading to a larger utilization gap. VGGNet and GTX 980Ti, Inception V3, and GTX 1080, NASNet and Tesla V100 are chosen as representatives for 2013, 2015, and 2018 respectively. All FLOPs are measured for single precision.

in each convolution becomes smaller. For example, the average floating-point operations (FLOPs) per convolution has decreased from 2330 MFLOPs/kernel in VGG to 82 MFLOPs/kernel in NASNet. This exacerbates the device’s under-utilization problem.

To address this problem, recent work explores *inter-operator parallelism* by executing multiple CNN operators in parallel guided by different heuristics (Tang et al., 2018; Jia et al., 2019b). For example, MetaFlow (Jia et al., 2019b) fuses multiple operators matching a specific pattern into a larger operator to increase operator granularity. Tang et al. (Tang et al., 2018) proposes a *greedy* strategy that directly executes all available CNN operators on CPU to maximize resource utilization. These approaches apply different heuristics to optimize local parallelization across a few CNN operators; however, such techniques do not lead to a *globally opti-*

^{*}Work down while interning at MIT HAN Lab. ¹University of Toronto ²Massachusetts Institute of Technology ³Carnegie Mellon University. Correspondence to: Song Han <songhan@mit.edu>.

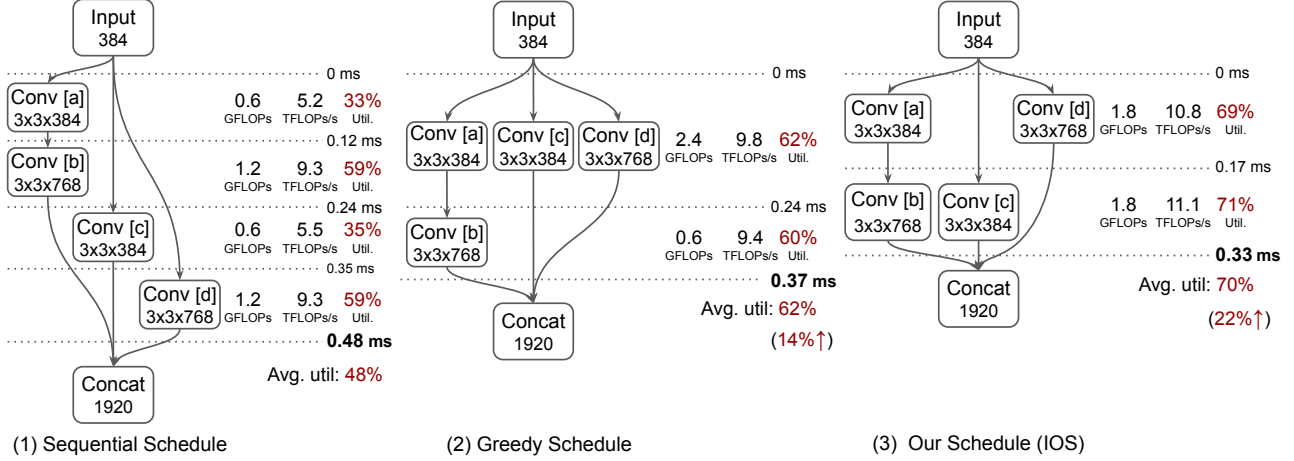


Figure 2. Different execution schedules for a computation graph on NVIDIA Tesla V100 GPU. Operators scheduled to run in parallel are placed at the same level between two dotted lines, which is called a *stage*. Computation (GFLOPs), performance (TFLOPs/s), and hardware utilization (%) for each stage are profiled on the right. Both sequential and greedy schedules result in low resource utilization (48%-62%) and high latency (0.37-0.48ms). Our schedule yields higher utilization (70%) and lower latency (0.33ms).

mal schedule for the entire CNN architecture. For example, given an input CNN (Figure 2 (1)), a greedy schedule (Figure 2 (2)) would perform convolutions [a], [c], and [d] in parallel, and run convolution [b] in a subsequent stage upon the completion of the previous stage.

This greedy schedule is sub-optimal for two reasons. First, a greedy schedule eagerly puts more operators in the early stages (as soon as they are available) and fewer operators in subsequent stages, resulting in low utilization in later stages. Second, executing too many operators on the device concurrently may lead to resource contention problem that hurts the performance. For example, as shown in Figure 2, the greedy schedule (2) suffers from resource contention problem in the first stage and low-utilization problem in the second stage, comparing to our proposed schedule (3).

Obtaining an optimized schedule to parallelize a CNN model is a challenging task. On the one hand, the number of schedules grows exponentially with the number of operators, making it infeasible to exhaustively evaluate all possible schedules. For example, a network with 33 operators can have 9.2×10^{22} number of feasible schedules. On the other hand, an optimal schedule also depends on hardware specifications and inference settings (e.g., batch size). A high-end GPU (e.g., Tesla V100) can efficiently execute a schedule with many operators in parallel, while a low-end GPU (e.g., Tesla K80) might suffer from resource contention using the same schedule. Also, a large batch size naturally offers more intra-operator parallelism, while a small batch size has a stronger need for inter-operator parallelization. Therefore, given a diverse set of CNN architectures, hardware, and inference settings, it is hard to devise an efficient schedule manually for all scenarios.

To address this challenge, we propose IOS, an inter-operator scheduler that accelerates CNN inference by combining intra- and inter-operator parallelism. We observe that different schedules share common sub-schedules; thus, IOS adopts a dynamic programming technique to explore the schedule space and finds a highly optimized schedule under low search cost. We evaluate IOS on modern CNN models, including Inception-V3 (Szegedy et al., 2016), RandWire (Xie et al., 2019), NasNet-A (Zoph et al.), and SqueezeNet (Iandola et al., 2016). IOS consistently outperforms the sequential schedule and greedy schedule. IOS achieves 1.1-1.5 \times inference speedup compared to existing deep learning libraries (e.g., TensorRT). Furthermore, IOS demonstrates the necessity of *customizing the scheduling policy* for different hardware and inference configurations. By customizing the scheduling recipe, IOS can achieve up to 1.15 \times inference speedup compared to itself with no customization. We will make IOS open-source upon publication.

Our contributions are summarized as follows:

- We point out a major bottleneck for efficient CNN inference: existing intra-operator parallelism cannot saturate modern hardware’s high parallelism, especially for recent multi-branch CNN models. Inter-operator parallelism is crucial.
- We propose a novel dynamic programming algorithm to find a highly optimized schedule for inter-operator parallelization. This technique is platform-agnostic and can serve as a general optimization for popular frameworks such as TensorFlow (Abadi et al., 2015) and TVM (Chen et al., 2018).

- We apply IOS to different hardware and inference settings and show that the different configurations require different schedules. We can automatically customize the scheduling policy for different hardware and inference configurations. The specialized schedules consistently outperform existing deep learning libraries with $1.1\text{-}1.5\times$ measured speedup in inference.

2 BACKGROUND AND RELATED WORK

CNN Design. A number of lightweight design primitives have been recently introduced to improve the efficiency of CNNs. Examples include SqueezeNet (Iandola et al., 2016), MobileNet (Sandler et al., 2018) and ShuffleNet (Zhang et al., 2018). However, such design patterns cannot fully utilize the hardware. Hardware under-utilization becomes more severe as accelerators are getting more powerful (shown in Figure 1). On the other hand, multi-branch CNNs become a trend in model architecture design, including both manually designed networks (Szegedy et al., 2015; Iandola et al., 2016; Szegedy et al., 2016) and the networks discovered by neural architecture search (Cai et al., 2018; Zoph et al.). With a fixed computation budget, multi-branch CNNs use more small convolution primitives, which further amplifies the resource under-utilization problem on modern hardware.

Intra-operator Parallelism. Current deep learning frameworks (e.g., TensorFlow and PyTorch) generally focus on intra-operator parallelism, which executes arithmetic operations within a *single* operator in parallel (e.g., tiled matrix multiplication). Tensorflow and PyTorch are built upon vendor-provided libraries (e.g., cuDNN), a set of DNN compute primitives heavily optimized by vendor engineers to achieve near-peak machine performance. However, these DNN operators are executed sequentially on a hardware device. The degree of parallelism within an operator is limited; thus, intra-operator parallelism cannot provide sufficient parallelizable computation to feed powerful hardware devices. As a result, the hardware is often under-utilized using these frameworks.

Different from manual performance tuning, AutoHalide (Mullapudi et al., 2016), TVM (Chen et al., 2018) and Ansor (Zheng et al., 2020) exploit intra-parallelism through automatically *learning* efficient schedule for individual DNN kernels. This automation saves a large amount of engineering effort and can generate more efficient DNN kernels compared to the manually designed counterparts. But still, all these libraries only focus on intra-operator parallelism but do not exploit inter-operator parallelism.

Greedy-based Inter-Operator Scheduling. The number of potential inter-operator schedules grows exponentially with the number of operators in a CNN. Tang et al. (Tang et al., 2018) propose a greedy heuristic approach that ex-

ecutes all available CNN operators whenever possible to saturate the computation capability in CPU. Though it keeps the otherwise idle cores busy, the greedy strategy suffers from resource contention due to limited shared resources such as the last-level cache in GPU. Besides, the greedy strategy does not optimize performance at the level of a *whole* computation graph and thus yields unbalanced and sub-optimal schedules.

Graph transformation. MetaFlow (Jia et al., 2019b) performs functional-preserving graph transformations to optimize DNN architectures. By merging operators with the same input, it enables more parallelism (a larger operator compared to two small sequential operators) and reduces accesses to GPU memories. TASO (Jia et al., 2019a) further introduces an automated generation of substitution rules and it explores more mathematically equivalent DNN architectures of the input one comparing to MetaFlow. MetaFlow and TASO can take the whole graph into consideration and search for high optimized substitution strategies. However, the inter-operator parallelism utilized by MetaFlow and TASO is still limited as only the same type of operators can be merged.

To address the large schedule space problem, IOS utilizes dynamic programming to take advantage of the common sub-schedules among different schedules. In addition, IOS also supports concurrent execution of different types of operators, addressing the limitation of MetaFlow and TASO.

3 PROBLEM DEFINITION

This section defines the *schedule* in IOS and formulates the problem.

Computation Graph. A CNN is defined by a computation graph $G = (V, E)$, where V is the set of operators, and E is the edge set representing dependencies. A computation graph is a directed acyclic graph (DAG). Each operator in the graph represents an operator such as convolution and matrix multiplication. Each edge (u, v) is a tensor that is an output of operator u and an input of operator v . Figure 3 (1) shows the computation graph of a simple CNN.

Stage. To take advantage of inter-operator parallelism in a CNN architecture, its computation graph is partitioned into multiple stages. Stages are executed sequentially and the operators in the same stage are executed according to a certain parallelization strategy (see below). Figure 3 (2) shows a possible schedule that partition the input graph into two stages, where the first stage contains operator a and b, and the second stage contains operator c, d, and e. The parallelization strategy is discussed below.

Parallelization Strategy. Each stage adopts one of the following two parallelization strategies: *operator merge* and

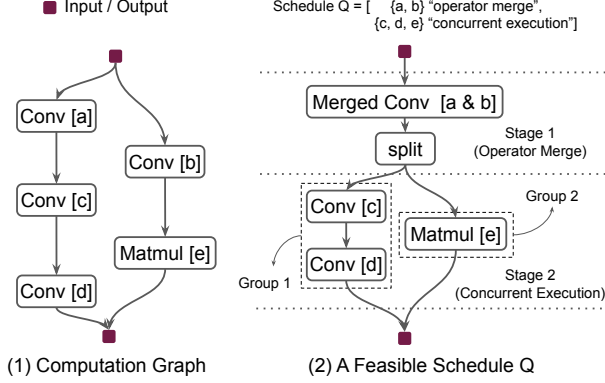


Figure 3. For a given *computation graph* (left), a possible *schedule* is shown to the right. There are five operators in the graph: convolutions a-d and matrix multiplication e. The schedule partitions operators into 2 *stages*. The first stage merges convolution a and b into a larger convolution, this parallelization strategy is named *operator merge*. The second stage partitions operator c, d and e into two *groups*, $\{c, d\}$ and $\{e\}$. The operators in the same group are executed sequentially while different groups in the same stage are executed concurrently. This parallelization strategy is named *concurrent execution*. Stages are executed one-by-one.

concurrent execution.

To be eligible for *operator merge*, the operators’ type must be the same while the hyperparameters can be different. For example, two convolutions with the same stride but different kernel sizes can also be merged. The smaller kernel will be padded with zeros to fit the large kernel so we can stack their kernels together. In Figure 3 (1), if Conv[a] has 128 3x3 kernels while Conv[b] has 256 3x3 kernels, we can stack their kernels together and replace Conv[a] and [b] by a Merged Conv[a&b] with 384 3x3 kernels. Besides increasing parallelism, it also reduces the memory accesses to the input tensor from twice to only once. A split operator is required to split the output of the merged convolution to recover the original outputs of Conv[a] and Conv[b].

Under *concurrent execution*, the operators in the stage are partitioned into disjoint *groups*. More specifically, if two operators are connected by an edge, they are partitioned into the same group. Different groups within the same stage are executed concurrently, while the operators within the same group are executed sequentially. IOS considers simultaneous executions of operators with *different* types. In the second stage of Figure 3 (2), the three operators are partitioned into two groups. The first group contains operator Conv[c] and Conv[d] while the second group contains operator Matmul[e]. The two groups are executed concurrently while Conv[c] and Conv[d] are executed sequentially in their group.

ISO considers both operator merge and concurrent execution and automatically picks the more efficient one for each stage. The choice depends on the operator types, the input

tensor shapes, and the hardware device to perform CNN computations. Section 7.1 provides a detailed case study to show the choices for different combinations of these factors.

Schedule. We define a *schedule* Q of a computation graph G as follows:

$$Q = \{(S_1, T_1), (S_2, T_2), \dots, (S_k, T_k)\}$$

where S_i is the set of operators in the i th stage and T_i is the corresponding parallelization strategy, either “concurrent execution” or “operator merge”. For example, the schedule for Figure 3 (2) is: $Q = \{(\{a, b\}, \text{operator merge}), (\{c, d, e\}, \text{concurrent execution})\}$. The schedule Q executes the network from the first stage (S_1, T_1) to the last stage (S_k, T_k) sequentially. S_i may contain only one operator if it is the best choice (e.g., a very large operator that saturates the entire GPU).

Problem Formulation. Let c be a cost function defined on a computation graph G and schedule Q . We aim to find a schedule Q^* to minimize the cost function for a given computation graph G , i.e., $Q^* = \text{argmin}_Q c(G, Q)$. In this work, the cost function $c(G, Q)$ is defined as the latency of running G following schedule Q .

4 METHODS

This section introduces our Inter-Operator Scheduler (IOS) in three parts. Section 4.1 elaborates the IOS design in details. Section 4.2 analyzes the time complexity of IOS. Finally, Section 4.3 introduces the pruning optimizations to further reduce the search time of IOS.

4.1 Inter-Operator Scheduler (IOS)

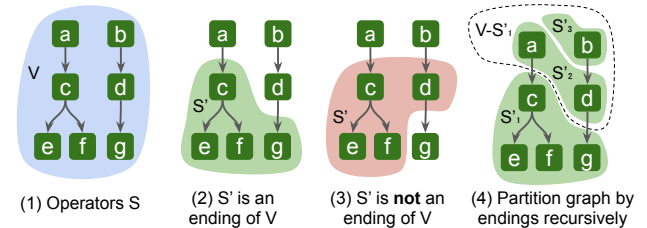


Figure 4. The illustration of *ending*. (1) shows all the operators S ($V=S$). S' in (2) is an ending of V . But S' in (3) is not an ending of V because there is an edge from d to g (from S' to $V-S'$). We can partition a graph by selecting an ending for remaining operators recursively, as shown in (4), where S'_1 is an ending of V while S'_2 is an ending of $V-S'_1$.

To find an optimized schedule for a CNN architecture, we first partition its computation graph $G = (V, E)$ into $V-S'$ and S' , where all edges between $V-S'$ and S' start from $V-S'$ and end in S' . Such S' is called an *ending* of V , as illustrated in Figure 4. There are many endings of V . The last stage operators in V ’s optimal schedule must be an

ending of V . We can enumerate the ending S' and convert the original problem to a sub-problem that finds the optimal schedule for $V - S'$. The whole graph can be scheduled by applying the partition recursively.

Let $\text{cost}[S]$ be the latency of an optimal schedule for S . Let $\text{stage_latency}[S']$ be the latency of stage (S', T) where T is the better parallelization strategy for S' among the two possible ones. We formalize this idea as following,

$$\text{cost}[S] = \min_{S'} (\text{cost}[S - S'] + \text{stage_latency}[S']),$$

where S' is an ending of S , and $\text{cost}[\emptyset] = 0$. Finally, $\text{cost}[V]$ is the latency of an optimal schedule for the entire computation graph G . To construct an optimal schedule, we record the corresponding S' that minimizes the latency for each S .

With this general idea, we implement IOS in three functions **INTEROPERATORSCHEDULER** (L3-12), **SCHEDULER** (L13-22) and **GENERATESTAGE** (L23-33) as shown in Algorithm 1. **INTEROPERATORSCHEDULER** takes a computation graph as an input and returns an optimized schedule found by IOS. **SCHEDULER** is a recursive function implementing the dynamic programming algorithm to find the optimal schedule for a subset of operators in G . **GENERATESTAGE** chooses a better parallelization strategy for given operators S' .

INTEROPERATORSCHEDULER (L3-12) is the entry function. It takes a computation graph G as an input and returns an optimized schedule Q . This function calls **SCHEDULER** with operators V as an argument (L5). After calling **SCHEDULER**, the global variable $\text{cost}[S]$ stores the latency of an optimal schedule for S , while $\text{choice}[S]$ stores the last stage in the corresponding optimal schedule. Once $\text{choice}[\cdot]$ is obtained, we can construct the schedule found by IOS (L6-11). We start with an empty list as the initial state of our schedule (L6) and let S be all the operators in G . We inquire about the last stage (S', T) of S by $\text{choice}[S]$ and put it at the head of the current schedule Q . We repeat this process by letting $S = S - S'$ to get the schedule for the remaining operators in all previous stages (L8-11). $S = \emptyset$ indicates that we have discovered an optimized schedule Q for G .

SCHEDULER (L13-22) is the core part of our algorithm. It implements the dynamic programming algorithm in a recursive manner, taking a subset of V as the state. It takes a set of operators S as an input and returns the minimal latency for S among all schedules. Because **SCHEDULER** may be called multiple times with the same argument S , for repeated calls, we directly return the previously cached result $\text{cost}[S]$ to avoid redundant computations (L14-15). To find an optimal schedule for S , we enumerate its last stage operators S' and reduce the problem into a sub-problem for $S - S'$ (L16-21). We use **GENERATESTAGE** to choose a better parallelization strategy $T_{S'}$ for S' and get the latency

Algorithm 1 Inter-Operator Scheduler (IOS)

Input: a computation graph $G = (V, E)$,
and a schedule pruning strategy P

Output: a schedule found by IOS

```

1: Let  $\text{cost}[S] = \infty$  for all  $S \subseteq V$  but  $\text{cost}[\emptyset] = 0$ 
2: Let  $\text{choice}[S] = \emptyset$  for all  $S \subseteq V$ 
3: function INTEROPERATORSCHEDULER( $G$ )
4:    $V =$  all operators in computation graph  $G$ 
5:   SCHEDULER( $V$ )
6:    $Q =$  empty list
7:    $S = V$ 
8:   while  $S \neq \emptyset$  do
9:      $S', T = \text{choice}[S]$ 
10:    Insert stage  $(S', T)$  before the head of  $Q$ 
11:     $S = S - S'$ 
12:   return the schedule  $Q$ 
13: function SCHEDULER( $S$ )
14:   if  $\text{cost}[S] \neq \infty$  then
15:     return  $\text{cost}[S]$ 
16:   for all ending  $S'$  of  $S$  satisfying pruning strategy  $P$  do
17:      $L_{S'}, T_{S'} = \text{GENERATESTAGE}(S')$ 
18:      $L_S = \text{SCHEDULER}(S - S') + L_{S'}$ 
19:     if  $L_S < \text{cost}[S]$  then
20:        $\text{cost}[S] = L_S$ 
21:        $\text{choice}[S] = (S', T_{S'})$ 
22:   return  $\text{cost}[S]$ 
23: function GENERATESTAGE( $S'$ )
24:   Partition  $S'$  into disjoint groups:  $S'_1, S'_2, \dots, S'_k$ .
25:    $L_{\text{concurrent}} =$  latency of parallel execution of  $\{S'_i\}$ 
26:   if operators in  $S'$  can be merged then
27:      $L_{\text{merge}} =$  latency of merged operator
28:   else
29:      $L_{\text{merge}} = \infty$ 
30:   if  $L_{\text{concurrent}} < L_{\text{merge}}$  then
31:     return  $L_{\text{concurrent}}$ , “concurrent execution”
32:   else
33:     return  $L_{\text{merge}}$ , “operator merge”
    
```

$L_{S'}$ (L17). L_S is the minimal latency for S in the case of taking S' as the last stage operators (L18). We enumerate all possible endings of S and record the minimal latency L_S and the corresponding last stage $(S', T_{S'})$ in $\text{cost}[S]$ and $\text{choice}[S]$, respectively (L19-21).

GENERATESTAGE (L23-33) chooses a better parallelization strategy from “concurrent execution” and “operator merge” for a given stage S' . It returns the parallelization strategy and the corresponding latency. It directly measures the latencies of both parallelization strategies on the hardware. For the “concurrent execution” strategy, it partitions S' into multiple disjoint operator groups: S'_1, S'_2, \dots, S'_k . Operators in different groups are executed concurrently while operators in the same group are executed sequentially. For the “operator merge” strategy, if all the operators in S' can be merged into a single operator (L26), we merge them and measure the latency of the merged operator (L27). Otherwise, we set L_{merge} to infinity to force to choose the “concurrent execution” strategy.

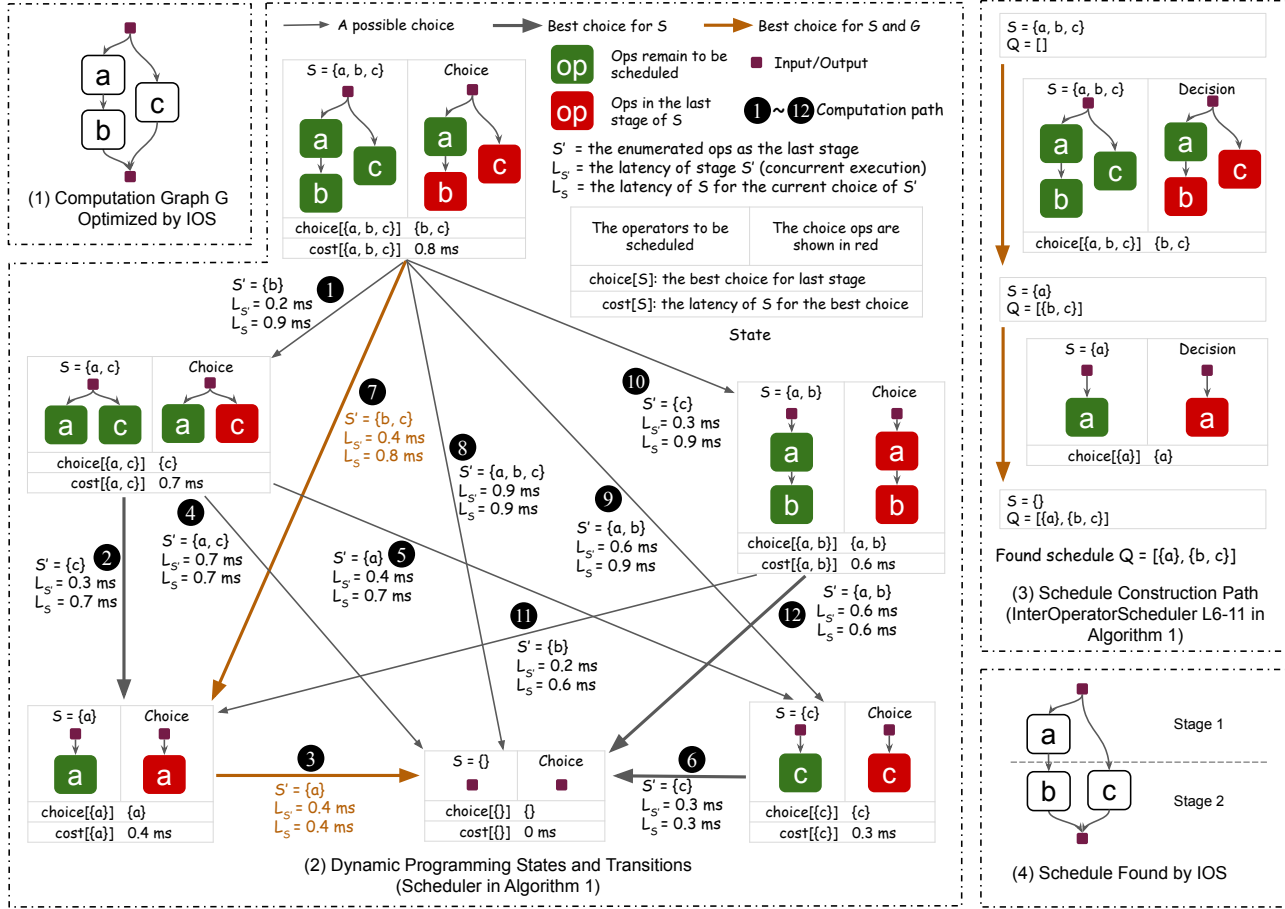


Figure 5. An example to illustrate how IOS finds the schedule. The computation graph to be optimized is shown in (1). It has three operators a , b , and c , where a is followed by b , and c is independent with a and b . The states and transitions between these states are presented in (2). Here *state* means the operators to be scheduled, and *transition* means the dependency between states (edges in (2)). Any path from state $S = \{a, b, c\}$ to $S = \{\}$ is corresponded with a schedule. Upon finishing the dynamic programming process (SCHEDULER), the best schedule for the computation graph can be constructed according to $choice[\cdot]$, as shown in (3). The schedule found by IOS is shown in (4). For simplicity, in this example, we only consider the concurrent execution parallelization strategy.

Figure 5 demonstrates how IOS discovers an optimized strategy for an input graph with three operators a , b , and c . Figure 5 (2) shows the dynamic programming process, the SCHEDULER in Algorithm 1. For simplicity, we only consider the concurrent execution parallelization strategy. There are six *states* (the operators to be scheduled, S) in the process. We start with all the operators in the computation graph as state $S = \{a, b, c\}$ (L5). For each state S , SCHEDULER enumerates the ending S' of S . The latency of S contains two parts: latency of S' as a stage and the latency of $S - S'$. While the result of S' is measured on the device directly ($L_{S'}$), the optimal latency of $S - S'$ is obtained via solving the sub-problem recursively. ① to ⑫ show the computation paths. Note that IOS memorizes the results for each calculated state to avoid redundant computations. Thus, step ⑦ visits state $S = \{a\}$ and IOS gets its latency directly (L15) because it has been previously visited by step ②. SCHEDULER stores the latency ($cost[\cdot]$) and last stage

($choice[\cdot]$) in its optimal schedule. We can construct the best schedule for the whole computation graph using $choice[\cdot]$, as shown in Figure 5 (3). An optimal schedule found by IOS is shown in (4). Both stages take “concurrent execution” as the parallelization strategy.

4.2 Time Complexity of IOS

In this subsection, we analyze the time complexity of IOS. We take set operations (L18, L24) and latency measurement operations (L25, L27) as atom operations to make the analysis more clear. To analyze the time complexity of IOS, we count the number of executions of L17-21, since they dominate the execution of the whole algorithm. This number equals the number of edges (i.e., transitions) in Figure 5 (2). Furthermore, it is equivalent to count the number of pairs (S, S'), where S is a state and S' is an ending of S . Here we define the width of a directed acyclic graph and provide the time complexity of Algorithm 1.

Definition 1 (Width d of a DAG). We call d the *width* of a directed acyclic graph G if we can find at most d operators in G such that there is no path connecting any two of them.

Theorem (Time Complexity of IOS). The time complexity of Inter-Operator Scheduler(IOS) is $\mathcal{O}(\binom{n/d+2}{2}^d)$, which can be relaxed to $\mathcal{O}((\frac{n}{d} + 1)^{2d})$, where n is the number of operators in the computation graph and d is its width.

In fact, there are computation graphs that can reach this bound, so we can not improve it without other restrictions on the schedule space. Proof can be found in Appendix A.

Model	n	d	$\binom{n/d+2}{2}^d$	$\#(S, S')$	#Schedules
Inception V3	11	6	2.6×10^4	4.9×10^3	3.8×10^6
Randwire	33	8	3.7×10^9	1.2×10^6	9.2×10^{22}
NasNet	18	8	5.2×10^6	3.1×10^5	7.2×10^{12}
SqueezeNet	6	3	2.2×10^2	51	1.3×10^2

Table 1. For the largest block of each benchmarked network, we list the number of operators n , the width d , the upper bound of transitions $\binom{n/d+2}{2}^d$, the real number of transitions $\#(S, S')$, and number of schedules.

Modern convolution neural networks usually construct the network by stacking multiple blocks, making it possible to optimize each block separately. In this case, n and d refers to the number of operators within a block and the block width, rather than the full network. We list the information of the largest block for each network benchmark in Table 1.

The total number of feasible schedules is exponential to the number of operators (e.g., up to 9.2×10^{22} for Randwire (Xie et al., 2019)). Such a huge number makes it prohibitive to manually design or enumerate the schedules. However, by reusing the results of common sub-schedules in the schedule finding process, IOS finds the optimal schedule within 4 hours for each network with no pruning strategy used. The time complexity of IOS is only exponential to the width of the computation graph, which is usually very small and acceptable (e.g., ≤ 8 in all benchmarked networks).

4.3 Reduce the Search Time by Schedule Pruning

It is difficult for a dynamic programming algorithm to stop early, because it gets the best result at the very end. To reduce the search time, IOS introduces *schedule pruning* to reduce the exploration space by restricting the max number of groups and the max number of operators within a group. We define the pruning strategy P as a boolean function of S and S' . We only enumerate the ending S' of S that satisfies the pruning strategy P , that is, $P(S, S') = \text{True}$ (L16 of Algorithm 1). The pruning strategy consists of two parameters r and s : $P(S, S') = \text{True}$ if and only if ending S' has at most s groups and each group has at most r operators.

After applying the pruning strategy P , the time complexity is reduced from $\mathcal{O}((\frac{n}{d} + 1)^{2d})$ to $\mathcal{O}((\frac{n}{d} + 1)^d(r + 1)^s)$. Of course, there is a trade-off between the search cost and the quality of the discovered schedule. We evaluate this trade-off in Section 7.2.

5 IMPLEMENTATION SETUP

IOS is a framework-agnostic algorithm and can be implemented in popular frameworks. We implement the dynamic programming scheduling algorithm in Python and the execution engine in C++. The latency of a stage is directly measured in the execution engine to guide the scheduling. The execution engine is based on vendor-provided library cuDNN(Chetlur et al., 2014) and supports the parallel execution of operators. To concurrently execute multiple groups of operators, IOS puts different groups into different CUDA streams. Kernels in different CUDA streams will be executed in parallel if there are enough computation resources.

In the experiment, we build IOS based on cuDNN 7.6.5, cuda 10.2 and NVIDIA driver 450.51.05. We adopt TensorRT 7.0.0.11 and TVM 0.7 as baseline libraries. All the experiments are conducted in NVIDIA Tesla V100, unless otherwise stated.

Networks	#Blocks	#Operators	Operator Type
Inception V3	11	119	Conv-Relu
Randwire	3	120	Relu-SepConv
NasNet	13	374	Relu-SepConv
SqueezeNet	10	50	Conv-Relu

Table 2. The CNN benchmarks. Number of blocks, number of operators and the main operator type for each network are listed in the table. Here “Conv-Relu” means a convolution followed by a ReLU activation and “Relu-SepConv” means ReLU activation followed by separable convolution.

We benchmarked four modern CNNs in the experiment: Inception V3 (Szegedy et al., 2016), RandWire (Xie et al., 2019), NasNet-A (Zoph et al.) and SqueezeNet (Iandola et al., 2016), as shown in Table 2. The number of blocks, number of operators, and main operator type for each network are listed in the table. IOS supports the user-defined schedule unit. In this experiment, we take the operator type shown in the table, besides other operators such as Concat, as the basic schedule unit.

We conduct each experiment 5 times and report the average performance. Because the schedule for each block is independent, IOS optimizes each block separately and combines the schedules for each block to get the whole network’s final schedule. We adopt the schedule pruning strategy with $r = 3$ and $s = 8$ in all experiments unless otherwise stated. The IOS optimization cost for Inception V3 and SqueezeNet is less than 1 minute and the IOS optimization cost for Randwire and NasNet is within 90 minutes.

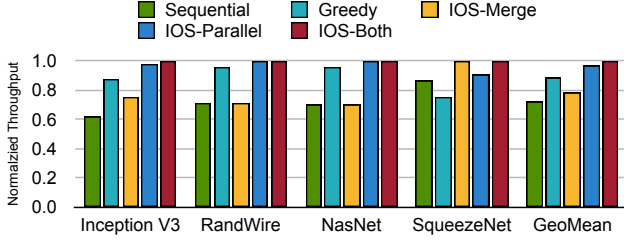


Figure 6. End-to-end performance comparison of different schedules across different CNNs on batch size one. The throughput is normalized to the best one for each model.

6 EXPERIMENTS

6.1 Comparison of Different Schedules

We first compare the inference performance among different schedules with batch size one. We compare five schedules: sequential schedule, greedy schedule, IOS-Merge schedule, IOS-Parallel schedule, and IOS-Both schedule, as shown in Figure 6. The sequential schedule is the schedule that executes the operator one-by-one according to certain topological ordering. The greedy schedule puts all the operators that can be executed currently in one stage, and repeats this process until all operators have been scheduled. IOS-Merge, IOS-Parallel, and IOS-Both schedules use the proposed approach to find the schedule but take different parallelization strategies. IOS-Merge only takes the “operator merge” strategy. IOS-Parallel only takes the “concurrent execution” strategy. IOS-Both considers both parallelization strategies. All schedules are executed on IOS execute engine for a fair comparison.

As shown in Figure 6, IOS-Both outperforms all the other four schedules. The greedy schedule gets good results on RandWire and NasNet. However, it degrades the performance of SqueezeNet because of the overhead of synchronization. Because we can not merge “Relu-SepConv” operators in RandWire and NasNet, IOS-Merge gets the same schedule as Sequential, and IOS-Both gets the same schedule as IOS-Parallel. IOS-Both considers two parallelization strategies and outperforms all the other four schedules. In later experiments, “IOS” refers to “IOS-Both” by default.

6.2 Comparison of cuDNN-based Frameworks

For popular frameworks, there are two ways to exploit the intra-operator parallelism. Frameworks such as Tensorflow (Abadi et al., 2015), TASO (Jia et al., 2019a), and TensorRT (NVIDIA) use the vendor-provided library cuDNN. Frameworks such as TVM (Chen et al., 2018) and Anso (Zheng et al., 2020) search the tensor program schedule for each kernel. TVM also provides support to call external libraries such as cuDNN to implement some kernels (e.g., convolution). In this subsection, we compare the perfor-

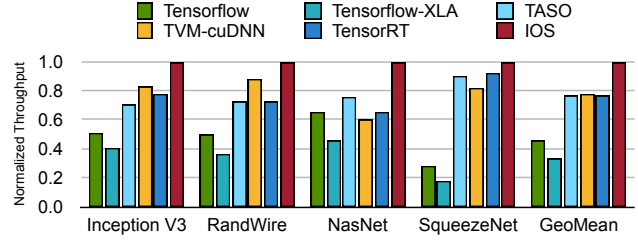


Figure 7. End-to-end performance comparison of different frameworks across different CNNs on batch size one. The throughput is normalized to the best one for each model.

mance of cuDNN-based frameworks with batch size one. Larger batch size is studied in the ablation study section.

As shown in Figure 7, there are five baselines: Tensorflow, Tensorflow-XLA, TASO, TVM-cuDNN, and TensorRT. Tensorflow-XLA is the tensorflow framework with XLA optimization turning on. TVM-cuDNN is the TVM framework that compiles a convolution neural network with cuDNN library, which would use the convolution kernel provided by cuDNN to execute convolutions. All other operators such as addition and concatenation would use their own kernels. For fair comparison, we only compare cuDNN-based libraries here, comparison between TVM-AutoTune and IOS can be found in the ablation study section. As shown in Figure 7, IOS consistently outperforms all five baseline frameworks on four benchmark CNNs. IOS can achieve $1.1\times$ to $1.5\times$ speedup comparing to the state of the art library TASO, TVM-cuDNN, and TensorRT.

6.3 Utilization Profiling

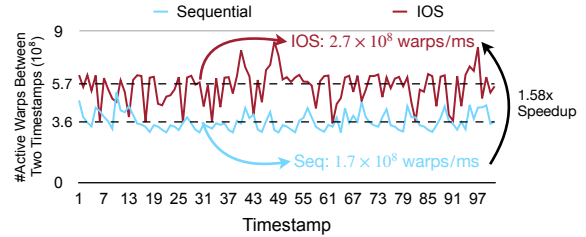


Figure 8. The profiling of active warps for networks in Figure 2 (a) and (c). Active warps indicates the number of actually executed instructions (1 warp = 32 inst.) on the device and can be used to show the device utilization. There is about 2.1 ms between two timestamps on average. IOS achieves higher device utilization (active warps/ms) than the sequential schedule.

We profiled two schedules in Figure 2 (1) and (3), using the CUDA profiling tools interface (CUPTI). We execute the computation graph repetitively and record the active warps between two sampling timestamps, which is proportional to the number of instructions executed.

The effective floating-point operations per second (FLOPS)

can be calculated by

$$\text{FLOPS} = w \frac{\text{warps}}{\text{ms}} \times 32 \frac{\text{threads} \cdot \text{cycle}}{\text{warp}} \times \frac{k \cdot \text{flop}}{\text{thread} \cdot \text{cycle}} \times 10^3 \frac{\text{ms}}{\text{sec}}$$

where w is the profiled metric: warps per millisecond (1.7×10^8 for sequential schedule and 2.7×10^8 for IOS schedule). The k in the formula is either 1 or 2 because FMA (fused multiply-addition) is counted as 2 FLOPs and many other float instructions are counted as 1 FLOP. Using this formula, we can get the FLOPS for sequential and IOS schedules are $5.5k$ TFLOPs/s and $8.7k$ TFLOPs/s. The single precision peak performance for NVIDIA Tesla V100 SXM2 (the one used in our experiment) is 15.7 TFLOPs/s and we can get the utilization of both schedules using the effective FLOPS to divide it. The utilization for sequential schedule and IOS schedule are 35% and 55% respectively, where $1 \leq k \leq 2$. The results in Figure 8 show that inter-operator parallelization increases the device utilization. This explains the reason of IOS speedup.

7 ABLATION STUDY

7.1 Specialized Scheduling is Beneficial

Specialization for Different Batch Sizes		Optimized for		
		1	32	128
Execute on	1	4.03	4.50	4.63
	32	29.21	27.44	27.93
	128	105.98	103.74	103.29

(1) Specialization for Batch Sizes

Specialization for Different Devices		Optimized for	
		K80	V100
Execute on	K80	13.87	14.65
	V100	4.49	4.03

(2) Specialization for Devices

Table 3. Latency (ms) of specialized schedules for batch size 1, 32 and 128, and specialized schedules for NVIDIA Tesla K80 and V100. The best performance is achieved when the schedule is specialized for each batch size and device. Each row is the batch size or device that the model is executed on. Each column is the batch size or device that IOS optimized for. InceptionV3 is used as benchmark.

Different workloads (e.g. network with different batch sizes) have different computation features, thus it is necessary to specialize the schedule for different workloads. We optimize Inception V3 with batch size 1, 32 and 128. Then we execute the network with these schedules on batch size 1, 32 and 128 separately, as shown in Table 3 (1). In Table 3 (1), the numbers in the same row represents the latency of the network executed with the same batch size but using schedules optimized for different batch sizes. The specialized schedule for each batch size achieved the best result.

To explore the specialization for different devices, we also optimize the network on both NVIDIA Tesla K80 and V100 with batch size one, as shown in Table 3 (2). The specialized schedule for each device also achieved better results.

IOS may discover different schedules for different batch sizes. For example, Figure 9 shows the schedule of the last

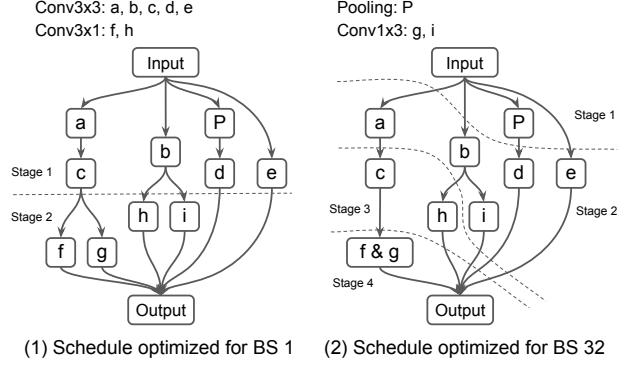


Figure 9. The schedule found by IOS for the last block of Inception V3. Operator a-e are convolution operator while operator P is the pooling operator. Schedule (1) and (2) are optimized for batch size 1 and 32 respectively. In schedule (1), there are two stages while in schedule (2) there are 4 stages. Schedule (1) is 28% faster than schedule (2) on batch size 1. Schedule (2) is 8% faster than schedule (1) on batch size 32.

block of Inception V3 optimized for batch size 1 and 32, respectively. There are two stages in the schedule (1), which is optimized for batch size 1 while there are four stages in the schedule (2), which is optimized for batch size 32. The schedule (1) is 28% faster than the schedule (2) on batch size 1, while the schedule (2) is 8% faster than (1) on batch size 32.

There are two differences between them. The first one is that convolution f and g in the schedule (2) are merged into a single convolution. This is because activation(the output tensor of an operator) is the memory bottleneck at large batch size. It's more crucial to reduce memory access, even at the cost of larger computation cost. Merging can reduce the memory access, because the merged kernel only access the output of convolution c once, instead of twice in the schedule (1). However, because the kernel size of f and g are 3x1 and 1x3 respectively, their kernel size would be expanded to 3x3 by padding zeros, which increase the amount of computation. Another difference between the schedule (1) and (2) is that the schedule (2) has more stages than the schedule (1). We found a similar phenomenon for large batch sizes. It is because of resource contention. When multiple operators are executed on the device, there is a conflict over access to the shared resources such as the last-level cache, making the concurrent execution degrades the performance. Resource contention gets more severe for larger batch sizes because the demand for shared resources gets larger.

7.2 Schedule Pruning Reduces Search Time

To explore the trade-off between optimized latency and optimization cost (i.e. search time), we optimize Inception V3 and NasNet with pruning strategy parameters $r = \{1, 2, 3\}$

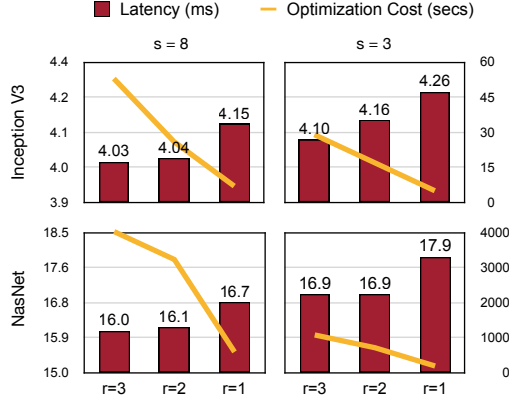


Figure 10. Trade-off between the optimized latency and the optimization cost for Inception V3 and NasNet. Two pruning strategy parameters r and s are used to prune the schedule space explored by IOS. r limits the maximum number of operators in each group while s limits the maximum number of groups in a stage. Left axis shows optimized latency and right axis shows the optimization cost.

and $s = \{3, 8\}$. As shown in Figure 10, when s and r get smaller, the optimization cost decreases at the cost of larger network latency. This is because smaller s and r restrict the schedules that IOS explores, thus reduce the optimization cost and increase schedule latency. By setting $r = 1$ and $s = 8$, IOS still achieves $1.59\times$ and $1.37\times$ speedup for Inception V3 and NasNet, comparing to sequential schedule. Meanwhile, the optimization cost for each network is within 30 seconds and 18 minutes, respectively.

7.3 Consistent Improvement for Different Batch Sizes

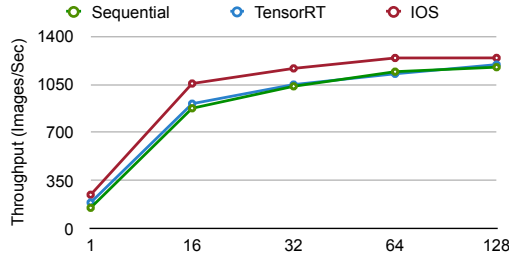


Figure 11. The throughput comparison of Sequential schedule, TensorRT and IOS on batch size 1, 16, 32, 64 and 128 for Inception V3.

In real-world applications, we need to handle different batch sizes for inference. For example, for real-time applications on edge devices, we usually use a batch size of 1 to reduce latency. In contrast, on cloud computing, the larger batch size is preferred to increase throughput. Changing the workload requires different inter-operator parallelization schedules. We optimize Inception V3 with batch size 1, 16, 32, 64, 128, and compare the throughput. As shown in Figure 11, the throughput increases when the batch size gets larger,

and when the batch size is larger than 128, the performance saturated and the throughput almost does not increase. The throughput of IOS outperforms the sequential schedule and TensorRT consistently on all batch sizes. Even though a larger batch size provides more data parallelism, we can still utilize inter-operator parallelism to further improve the throughput.

7.4 Intra- and Inter-Operator Parallelism

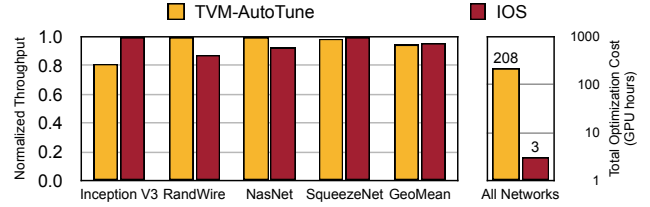


Figure 12. End-to-end performance comparison between TVM-AutoTune and IOS. TVM-AutoTune and IOS are *orthogonal* because TVM focuses on the intra-operator parallelism while IOS focuses on inter-operator parallelism. They can be combined to further boost the inference performance. The optimization cost of IOS is two orders of magnitude less than TVM.

TVM exploits the intra-operator parallelism by searching the schedule for each kernel on a specific device. IOS focuses on inter-operator parallelism and leaves the exploitation of intra-operator parallelism to cuDNN library. Although intra- and inter-operator parallelism is *orthogonal* and can be combined, we compare TVM and IOS here to give some insight into the benefit of each parallelism. We set the maximum trial number of schedules 2000 for each kernel, as suggested by TVM. TVM takes 208 GPU hours while IOS only takes 3 GPU hours in total to optimize the four networks. As shown in Figure 12, IOS outperforms TVM on Inception V3 and SqueezeNet. This is because only utilizing intra-parallelism can not provide enough parallelism for the powerful computing device. Meanwhile, TVM outperforms IOS on Randwire and NasNet. This is because TVM finds more efficient kernels for separable convolutions, which occupy the majority of operators in Randwire and NasNet. We believe the combination of TVM and IOS would boost the performance further. We leave this for future work.

8 CONCLUSION

With the increasing computational capacity, the sequential execution of CNNs no longer provides sufficient parallelization opportunities to fully utilize all the computation resources. We propose IOS that combines intra- and inter-operator parallelism and adapt dynamic programming to find an efficient schedule that better utilizes the hardware. Experiments show that IOS can improve the GPU utilization and speedup modern CNN inference from 1.1 to $1.5\times$ compared to the state-of-the-art libraries (e.g., TensorRT).

REFERENCES

- Abadi, M., Agarwal, A., Barham, P., Brevdo, E., Chen, Z., Citro, C., Corrado, G. S., Davis, A., Dean, J., Devin, M., Ghemawat, S., Goodfellow, I., Harp, A., Irving, G., Isard, M., Jia, Y., Jozefowicz, R., Kaiser, L., Kudlur, M., Levenberg, J., Mané, D., Monga, R., Moore, S., Murray, D., Olah, C., Schuster, M., Shlens, J., Steiner, B., Sutskever, I., Talwar, K., Tucker, P., Vanhoucke, V., Vasudevan, V., Viégas, F., Vinyals, O., Warden, P., Wattenberg, M., Wicke, M., Yu, Y., and Zheng, X. TensorFlow: Large-scale machine learning on heterogeneous systems, 2015. URL <http://tensorflow.org/>. Software available from tensorflow.org.
- Abadi, M., Barham, P., Chen, J., Chen, Z., Davis, A., Dean, J., Devin, M., Ghemawat, S., Irving, G., Isard, M., et al. Tensorflow: A system for large-scale machine learning. In *12th {USENIX} Symposium on Operating Systems Design and Implementation ({OSDI} 16)*, pp. 265–283, 2016.
- Cai, H., Yang, J., Zhang, W., Han, S., and Yu, Y. Path-level network transformation for efficient architecture search. In *ICML*, 2018.
- Chen, T., Moreau, T., Jiang, Z., Zheng, L., Yan, E., Shen, H., Cowan, M., Wang, L., Hu, Y., Ceze, L., et al. {TVM}: An automated end-to-end optimizing compiler for deep learning. In *13th {USENIX} Symposium on Operating Systems Design and Implementation ({OSDI} 18)*, pp. 578–594, 2018.
- Chetlur, S., Woolley, C., Vandermersch, P., Cohen, J., Tran, J., Catanzaro, B., and Shelhamer, E. cudnn: Efficient primitives for deep learning. *arXiv preprint arXiv:1410.0759*, 2014.
- Devlin, J., Chang, M., Lee, K., and Toutanova, K. BERT: pre-training of deep bidirectional transformers for language understanding. *CoRR*, abs/1810.04805, 2018. URL <http://arxiv.org/abs/1810.04805>.
- Dilworth, R. P. A decomposition theorem for partially ordered sets. *Annals of Mathematics*, 51(1):161–166, 1950. ISSN 0003486X. URL <http://www.jstor.org/stable/1969503>.
- Han, S., Mao, H., and Dally, W. J. Deep compression: Compressing deep neural networks with pruning, trained quantization and huffman coding. *arXiv preprint arXiv:1510.00149*, 2015.
- He, K., Zhang, X., Ren, S., and Sun, J. Deep residual learning for image recognition. In *Proceedings of the IEEE conference on computer vision and pattern recognition*, pp. 770–778, 2016.
- Iandola, F. N., Han, S., Moskewicz, M. W., Ashraf, K., Dally, W. J., and Keutzer, K. Squeezenet: Alexnet-level accuracy with 50x fewer parameters and 0.5 mb model size. *arXiv preprint arXiv:1602.07360*, 2016.
- Jia, Z., Padon, O., Thomas, J., Warszawski, T., Zaharia, M., and Aiken, A. Taso: Optimizing deep learning computation with automatic generation of graph substitutions. In *Proceedings of the 27th ACM Symposium on Operating Systems Principles, SOSP ’19*, pp. 47–62, New York, NY, USA, 2019a. Association for Computing Machinery. ISBN 9781450368735. doi: 10.1145/3341301.3359630. URL <https://doi.org/10.1145/3341301.3359630>.
- Jia, Z., Thomas, J., Warszawski, T., Gao, M., Zaharia, M., and Aiken, A. Optimizing dnn computation with relaxed graph substitutions. In Talwalkar, A., Smith, V., and Zaharia, M. (eds.), *Proceedings of Machine Learning and Systems*, volume 1, pp. 27–39. 2019b.
- Krizhevsky, A., Sutskever, I., and Hinton, G. E. Imagenet classification with deep convolutional neural networks. In *Advances in neural information processing systems*, pp. 1097–1105, 2012.
- Mnih, V., Kavukcuoglu, K., Silver, D., Graves, A., Antonoglou, I., Wierstra, D., and Riedmiller, M. Playing atari with deep reinforcement learning. *arXiv preprint arXiv:1312.5602*, 2013.
- Mullapudi, R. T., Adams, A., Sharlet, D., Ragan-Kelley, J., and Fatahalian, K. Automatically scheduling halide image processing pipelines. *ACM Transactions on Graphics (TOG)*, 35(4):1–11, 2016.
- NVIDIA. Nvidia tensorrt: Programmable inference accelerator. URL <https://developer.nvidia.com/tensorrt>.
- Paszke, A., Gross, S., Chintala, S., Chanan, G., Yang, E., DeVito, Z., Lin, Z., Desmaison, A., Antiga, L., and Lerer, A. Automatic differentiation in pytorch. In *NIPS-W*, 2017.
- Sandler, M., Howard, A., Zhu, M., Zhmoginov, A., and Chen, L.-C. Mobilenetv2: Inverted residuals and linear bottlenecks. In *Proceedings of the IEEE Conference on Computer Vision and Pattern Recognition*, pp. 4510–4520, 2018.
- Silver, D., Huang, A., Maddison, C. J., Guez, A., Sifre, L., Van Den Driessche, G., Schrittwieser, J., Antonoglou, I., Panneershelvam, V., Lanctot, M., et al. Mastering the game of go with deep neural networks and tree search. *nature*, 529(7587):484, 2016.

- Sutskever, I., Vinyals, O., and Le, Q. V. Sequence to sequence learning with neural networks. In *Advances in neural information processing systems*, pp. 3104–3112, 2014.
- Szegedy, C., Liu, W., Jia, Y., Sermanet, P., Reed, S., Anguelov, D., Erhan, D., Vanhoucke, V., and Rabinovich, A. Going deeper with convolutions. In *Proceedings of the IEEE conference on computer vision and pattern recognition*, pp. 1–9, 2015.
- Szegedy, C., Vanhoucke, V., Ioffe, S., Shlens, J., and Wojna, Z. Rethinking the inception architecture for computer vision. In *Proceedings of the IEEE conference on computer vision and pattern recognition*, pp. 2818–2826, 2016.
- Tang, L., Wang, Y., Willke, T. L., and Li, K. Scheduling computation graphs of deep learning models on manycore cpus. *arXiv preprint arXiv:1807.09667*, 2018.
- Xie, S., Kirillov, A., Girshick, R., and He, K. Exploring randomly wired neural networks for image recognition. *arXiv preprint arXiv:1904.01569*, 2019.
- Zhang, X., Zhou, X., Lin, M., and Sun, J. Shufflenet: An extremely efficient convolutional neural network for mobile devices. In *Proceedings of the IEEE Conference on Computer Vision and Pattern Recognition*, pp. 6848–6856, 2018.
- Zheng, L., Jia, C., Sun, M., Wu, Z., Yu, C. H., Haj-Ali, A., Wang, Y., Yang, J., Zhuo, D., Sen, K., Gonzalez, J. E., and Stoica, I. Ansor: Generating high-performance tensor programs for deep learning. In *14th USENIX Symposium on Operating Systems Design and Implementation (OSDI 20)*, Banff, Alberta, November 2020. USENIX Association. URL <https://www.usenix.org/conference/osdi20/presentation/zheng>.
- Zoph, B., Vasudevan, V., Shlens, J., and Le, Q. V. Learning transferable architectures for scalable image recognition. In *IEEE conference on computer vision and pattern recognition*.

A PROOF OF TIME COMPLEXITY

In this section of appendix, we prove the time complexity bound given in Section 4.2. In Section A.1, we give some preliminary definitions and theorems used in our proof. In Section A.2, we prove the time complexity of inter-operator scheduler (IOS).

A.1 Preliminary Definitions and Theorems

In this subsection, we give the definition of chain and anti-chain, Dilworth's theorem (Dilworth, 1950), and a corollary, which is used in our proof later.

Definition 2 (Chain and antichain). A *chain* is a subset of a partially ordered set such that any two distinct elements in the subset are comparable. An *antichain* is a subset such that any two distinct elements in the subset are incomparable.

Definition 3 (Chain decomposition of partial order set). A *chain decomposition* of a partial order set is a partition of the elements of the order into disjoint chains.

Theorem (Dilworth's Theorem). In any finite partially ordered set, the largest antichain has the same size as the smallest chain decomposition.

We apply the Dilworth's theorem to a directed acyclic graph and can get the following corollary.

Corollary 1. Let $G = (V, E)$ be a directed acyclic graph and d be the width of G . We can decompose V into d sets such that any two vertices in the same set can be connected by a path in G .

Proof. Let $P = (V, E')$ be the partial order derived from G by transitive closure. Then two elements u, v in V are comparable in P is equivalent to that there is a path between them in G . Thus, the width d of G equals the size of largest antichain of P . We apply the Dilworth's Theorem to P and can get a decomposition of V into d chains in P : S_1, S_2, \dots, S_d . Because S_i is a chain in P , any two elements in S_i are comparable, which means there is a path bridge them in G . \square

A.2 Time Complexity of Inter-Operator Scheduler

In this subsection, we will prove the time complexity of IOS stated in Section 4.2. Then we will show that the upper bound can be reached by some computation graph.

Lemma 1. If S'_1 ends S and S'_2 ends $S - S'_1$, then $S'_1 \cup S'_2$ also ends S .

Proof. We prove it by contradiction. If $S'_1 \cup S'_2$ does not end S , there must exist $(u, v) \in E$ such that $u \in S'_1 \cup S'_2$ and $v \in S - S'_1 \cup S'_2$. Then we have $u \in S'_1$ or $v \in S'_2$. If $u \in S'_1$, we can get the contradiction that S'_1 is not an ending of S because $v \in S - S'_1 \cup S'_2 \subseteq S - S'_1$. If $u \in S'_2$,

we can also get the contradiction that S'_2 is not an ending of $S - S'_1$ because $v \in S - S'_1 \cup S'_2 = (S - S'_1) - S'_2$. \square

Lemma 2. Let S be a possible argument of SCHEDULER, we have $V - S$ ends V .

Proof. We can rewrite S as $S = V - \bigcup_{i=1}^m S'_i$, where $m \geq 0$ and S'_k ends $V - \bigcup_{i=1}^{k-1} S'_i$ according to L17 in Algorithm 1. By repeatedly apply Lemma 1, we can get that $\bigcup_{i=1}^m S'_i$ ends V , which means $V - S$ ends V . \square

Lemma 3. Let V' be a subset of V and any two operators in V' are bridged by a path. Let c be the size of V' . Then

$$|\{(S \cap V', S' \cap V') \mid S' \text{ ends } S, V - S \text{ ends } V\}| = \binom{c+2}{2}$$

Proof. Because any two operators in V' is bridged by a path in G , operators in V' are ordered sequentially. Because $V - S$ ends V , there are only $c + 1$ possible sets of $S \cap V'$ because S must be a prefix in the sequential ordered operators, including empty set. $S' \cap V'$ is a suffix of $S \cap V'$, including empty set. Then there are $\sum_{i=0}^c \sum_{j=0}^i 1 = \frac{(c+2)(c+1)}{2} = \binom{c+2}{2}$ possible pairs of $(S \cap V', S' \cap V')$. \square

Theorem. The time complexity of inter-operator scheduler is $\mathcal{O}(\binom{n/d+2}{2}^d)$, which can be relaxed to $\mathcal{O}((\frac{n}{d} + 1)^{2d})$, where n is the number of operators in the computation graph and d is the width of it.

Proof. We only need to count the number of pairs of (S, S') that can reach L17 of Algorithm 1 because L17-21 dominates the execution time of the scheduler, where S is a subset of V that is taken as the argument of SCHEDULER and S' is an ending of S . By Lemma 2, $V - S$ ends V . By Corollary 1, we can decompose V into d disjoint partitions V_1, V_2, \dots, V_d and any two operators u, v in the same partition can be bridged by a path in G . We can build a one-to-one mapping that maps pair (S, S') to $2d$ -dimension tuple $(S \cap V_1, S' \cap V_1, \dots, S \cap V_d, S' \cap V_d)$ based on the partition. Then we only need to count the number of valid tuples to get the number of valid pairs. By Lemma 3, the possible number of pairs $(S \cap V_i, S' \cap V_i)$ is $\binom{c_i+2}{2}$. Then an upper bound of the tuples is $\prod_{i=1}^d \binom{c_i+2}{2}$. It is an upper bound but not the exact number because currently we only consider the dependency inside each partition V_i and ignored the dependency between different partitions. So the upper bound of the number of pairs of (S, S') is $\prod_{i=1}^d \binom{c_i+2}{2}$. It can be relaxed to $\binom{n/d+2}{2}^d$ because $\sum_{i=1}^d c_i = n$ and it is maximized when c_i are equal. For simplicity, it can further relaxed to $(\frac{n}{d} + 1)^{2d}$. \square

Here is an example to demonstrate that the time complexity of $\mathcal{O}(\binom{n/d+2}{2}^d)$ can be reached.

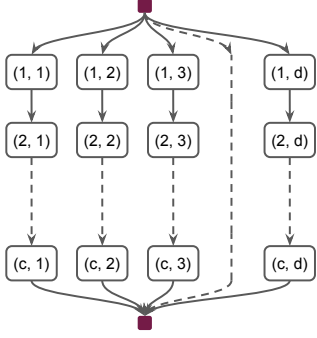


Figure 13. The example to make the time complexity $\mathcal{O}\left(\binom{n/d+2}{2}^d\right)$ tight. The time complexity for this graph is $\mathcal{O}\left(\binom{c+2}{2}^d\right)$

In this example, there are d independent paths and each path has c operators. Because the paths are independent with each other and there is no edge between two different paths, we can get the upper bound $\mathcal{O}\left(\binom{c+2}{2}^d\right)$ by the analysis in above time complexity proof.

B BLOCK-WISE SPEEDUP

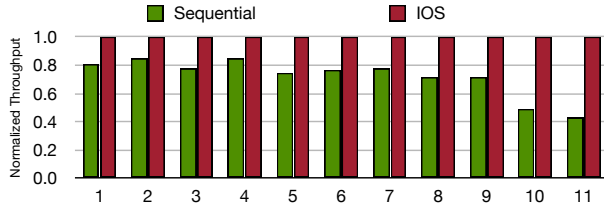


Figure 14. IOS consistently outperforms sequential executions on each block of Inception-v3.

To explore the speedup for different blocks, we compare the performance of each block of Inception-V3 (Szegedy et al., 2016) between sequential and IOS schedule (Figure 14). IOS consistently runs faster than the sequential schedule. The speedup for the individual block is up to $2.3\times$, and the end-to-end speedup is $1.6\times$. More speedup is achieved for back blocks because the width gets larger and more inter-parallelism is possible.